Recent upgrades to seismic physical modelling

Kevin L. Bertram and Joe Wong

ABSTRACT

A new, more robust water tank with reinforced acrylic sides was built for the Seismic Physical Modelling Laboratory. We characterized the wavelet shapes and 2D radiation patterns of three types of transducers operating in water in order to evaluate their effectiveness for producing low-frequency data suitable for efficient FWI. We designed and produced an Arbitrary Waveform Generator and evaluated its use for producing source-driving functions more complicated than simple impulses.

INTRODUCTION

Water-filled tanks are used for scale modelling of seismic acquisition in marine environments. Older versions of such a tank in the Seismic Physical Modeling Laboratory were built of wood and thin acrylic sheets were inadequate because they were not leak-proof. In the long term, they were unable to withstand the pressure of the required volume of water and developed cracks at the bottom. A replacement water tank with reinforced acrylic sides was designed and built to resolve both issues.

Efficient full-waveform inversion (FWI) imaging of complex velocity structures requires seismic data with low dominant frequencies in the range of 4Hz to 10Hz. When immersed in water in the laboratory, piezoelectric buzzers on will generate and detect vibrations with low-end ultrasonic frequencies ranging from 30kHz to 100kHz, so physically-modelled seismograms recorded with buzzer transducers will have the low frequencies (after applying a scaling factor of 10^4) required for seismic FWI. However, due to resonance effects in the buzzers, the seismogram codas are too long and too variable for them to serve as ideal FWT source wavelets. Finding ways to mitigate these two unfavorable characteristics is an ongoing task in our research in physical modelling

PART A: NEW WATER TANK

In 2018 CREWES had a water tank built with rather thin acrylic sheets for the physical modelling system to replace the old wooden tank. The goal was to maximize the size of the tank in an effort to minimize the effects of reflections from the tank sides and bottom on the acquired data. This 2018 tank was made from a three-quarter-inch-thick acrylic sheet on the bottom with half-inch-thick acrylic sheets for the sides.

The tank looked great, but there was a miscommunication during the manufacturing process. None of the screws that were used to hold the tank together were countersunk, and there were too few screws used As a result when the tank was placed on a cart and filled with water too much pressure was placed on the screw heads contacting the cart. Although this didn't damage the acrylic it did cause the silicone around the inside edges to become separated from the acrylic, which caused a leak. After this was discovered the tank was emptied and disassembled. All the screw holes were countersunk and countersunk screws were used to replace the button head screws. With the tank completely disassembled the opportunity was taken to add acrylic glue and methylene chloride to solidify the tank. Once completed the tank was put back into operation.

However, another problem presented itself in that the long sides of the tank would bow out when the tank was filled with water. Although the tank seemed stable in this bowed state it was a concerning sight to behold. To minimize this effect some square steel tubing and threaded rod were used to form a brace around the outside of the tank. Because the tank was designed to use the maximum space under the gantry system there wasn't space to put this bracing on the tank and slide it in place. Instead the tank had to be positioned under the gantry system first and then the bracing installed. There was still some bowing, but it was not as drastic as before.

The tank worked like this for two years. The tank is not left unattended for long periods of time with water in it, so a pump designed to empty a swimming pool is used to drain the water back into the sink drain. One morning while the tank was being refilled there was some audible cracking. The tank developed some leaks along one of the long sides. Even though the bowing out of the sides was reduced by the exterior brace the movement of the sides from full to empty and back again had caused the acrylic to crack above some of the screws in the long side (see Figure A1).

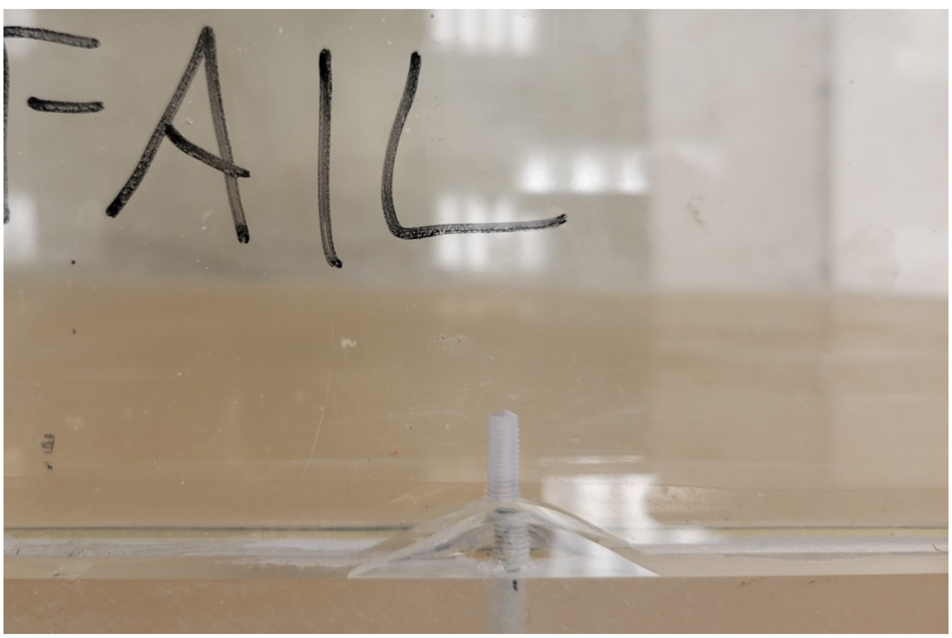

FIG. A1. Repeated movement caused a crack where a screw was used to hold the long side of the tank to the base of the tank. Multiple cracks of this type necessitated the construction of a new tank.

The failure of the 2018 tank meant that, firstly, a new, more robust tank needed to be built. Secondly, a method of detecting and containing a flood on the laboratory floor should be put in place should the tank fail while no one is present.

The previous tank was made from acrylic that was too thin to properly contain the amount of water required for the system. The sides of the tank were made of half-inch-thick acrylic and the base was three-quarter-inch-thick acrylic. These thicknesses were chosen to keep the weight and material costs to a minimum. We decided that the new tank should be made of one-inch-thick acrylic for both the base and the sides. Furthermore, the sides should be braced using three sets of four inch wide one inch acrylic wrapped around the outside of the tank. All the acrylic pieces should be bonded together chemically. The bottom bracing strips should cover the jointed edge around the bottom. The initial design can be seen in Figure A2.

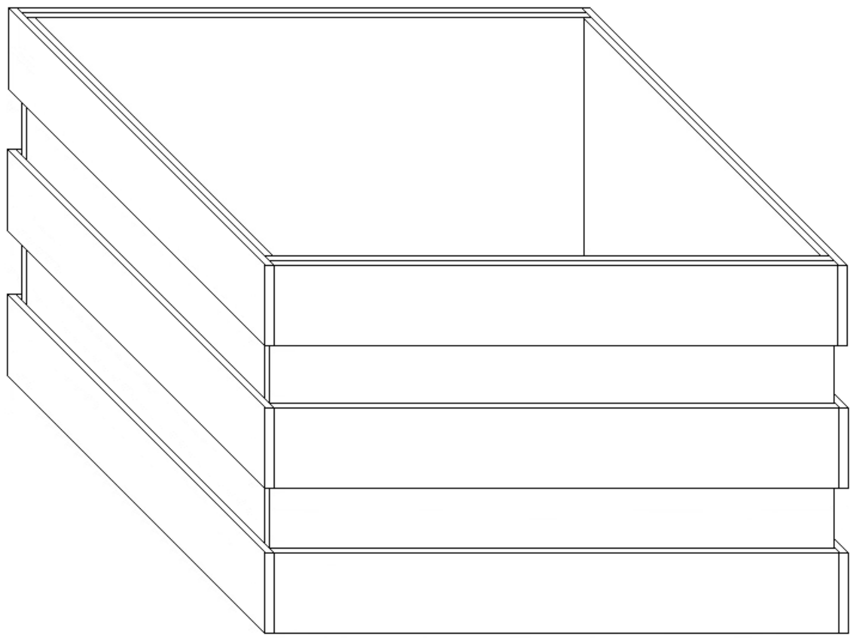

FIG. A2. The initial drawing for the new tank design.

The tank is designed using the same maximum outside dimensions. With the material now being an inch thick on all sides and another inch thick of bracing around that the interior volume is slightly smaller. The previous tank could hold a maximum of 600 litres whereas the new one can only hold 543 litres. This is an acceptable trade-off for a stronger tank.

We also decided to increase the number of screws used to hold the tank together. The hope here is that with more screws the load created by filling the tank with water can be distributed across more points to minimize the potential of failure. This time all the hardware was countersunk into the acrylic. The acrylic sheets needed for the new tank were ordered in the form of cut to size pieces with tapped screw holes for connections. All the machining was performed by the U of C Science Workshop and then delivered to CREWES for assembly (Figure A3). The tank was assembled by screwing the pieces together. A syringe applicator was then used to wick methylene chloride into all the joints. This “melts” the acrylic fusing the edges together and closing gaps that would leak.

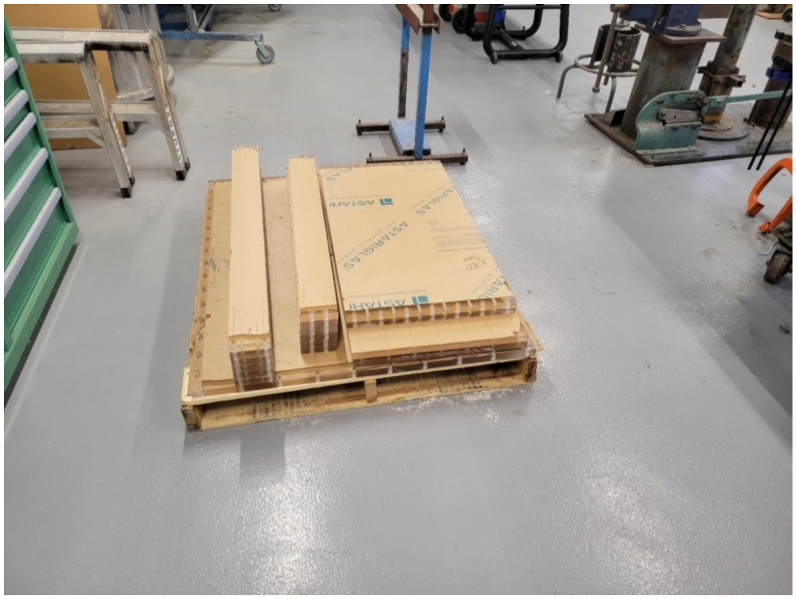

FIG. A3. The separate acrylic side and bottom sheets, ready to be assembled.

FIG. A4. The newly assembled and chemically bonded tank, after a weekend holding water near a floor drain. **The tank did not leak.**

The tank was assembled in a lab with a floor drain, filled with water, and left over the drain for a weekend (Figure A4). No leaks occurred, so it was emptied and dried. Silicone was applied to all the joints as another line of defense against leaking. On Figure A5, the now completed tank is seen placed under the Physical Modeling System automatic positioning subsystem.

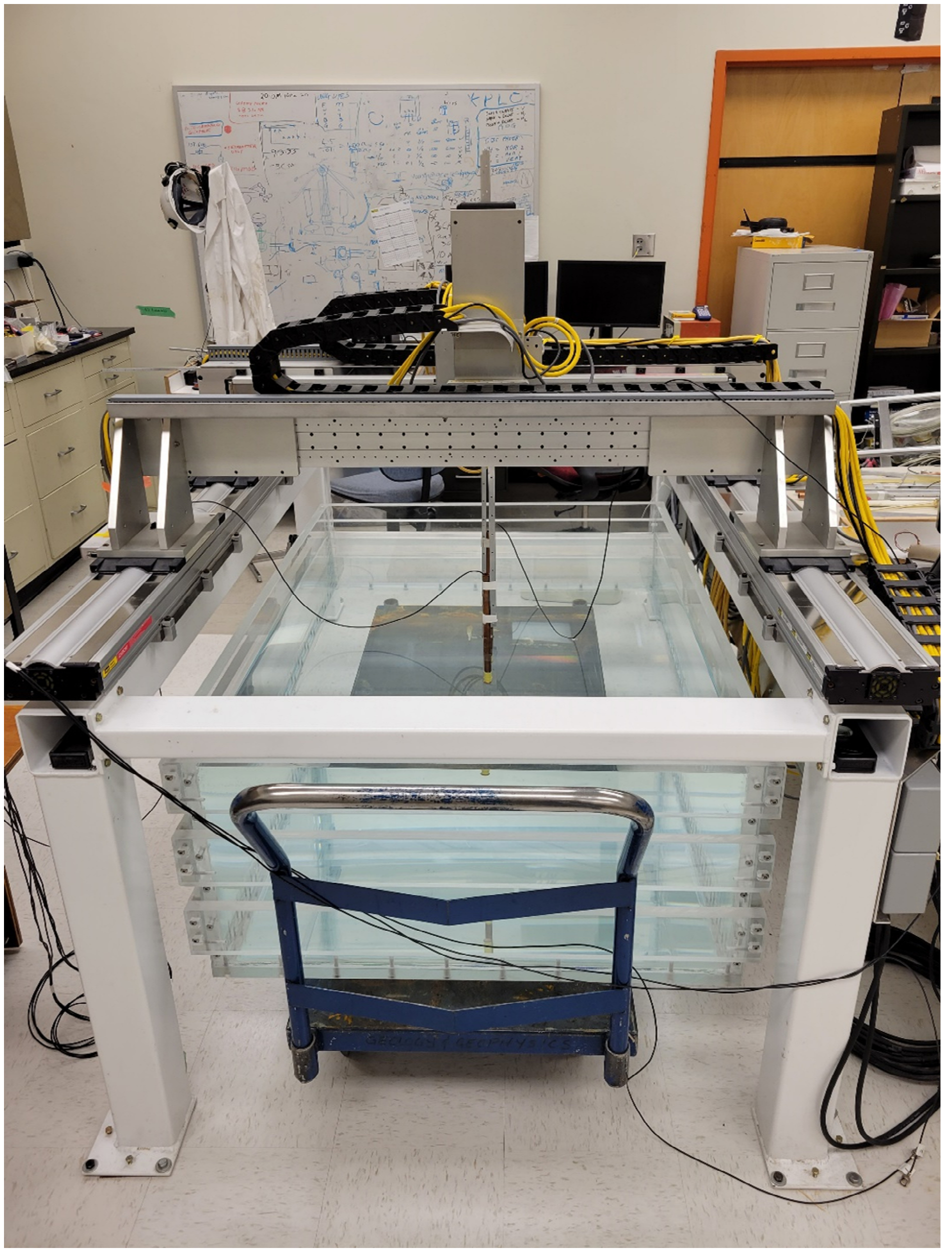

FIG. A5. The tank under the positioning gantries of the Physical Modelling System.

A method for containing and detecting a flood on the laboratory floor

Knowing that a leak is always possible a plan was now needed to deal with any leaks. It was decided to set up a berm around the tank and the gantry legs to contain any water that could potentially leak out of the tank. We decided to extend the berm past the end of the gantry system where the tank and its cart are moved in and out. This means that there is no need to have an end that opens to get the tank in and out. It also provides the advantage that a lower height berm could be used to contain the same volume of water. Required waterproofing of the floor and the legs holding up the positioning gantries would be accomplished by using waterproof tape.

With a containment system designed, the next step was to set up an automated system to deal with an unattended leak and subsequent flooding of the laboratory floor. The goal is to have this system do two things. The first is to alert select people via email that the tank has failed, and the second is to deal with the water within the containment system.

To manage these tasks, we decided to incorporate a Raspberry Pi single board computer in the flood mitigation efforts, FIGURE. By using the on board general purpose inputs and outputs (GPIO) both a water sensor to detect water in the berm and a relay to turn on a pump can be monitored and controlled.

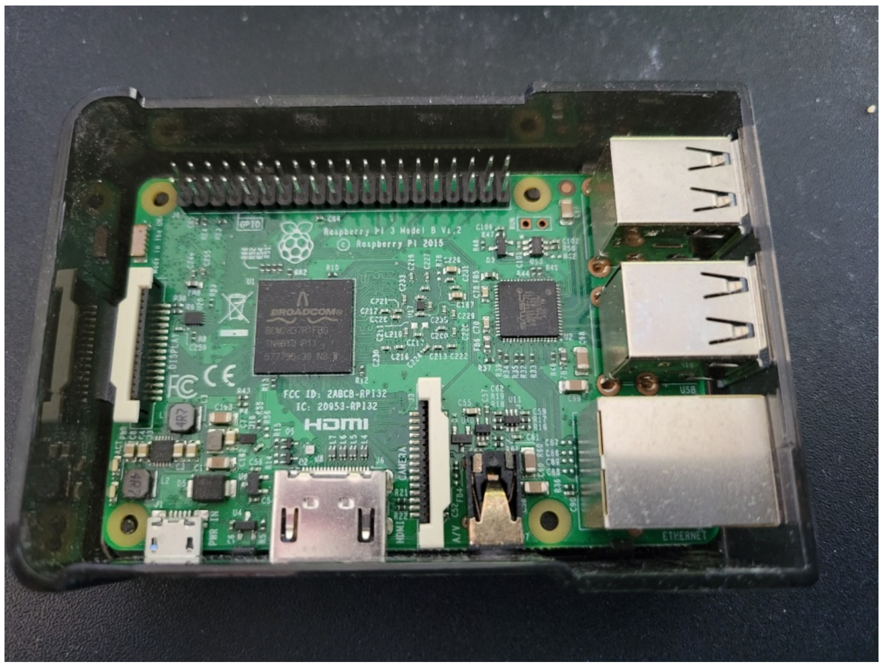

FIG. A6. A Raspberry Pi single board computer. The GPIO pins are at the top in this picture.

The first step was to set up a monitoring/detection method for water. We first considered a water sensor using strips of conductive material that completes a transistor circuit in the presence of water (Figure A7). Initial testing of this circuit was done using tap water and a microprocessor. This worked well. However, the physical modeling system does not use tap water in the tank. Demineralized water, which is available in most U of C labs, is used instead. Demineralized water is not electrically conductive, and so the sensor shown on Figure A7 would not work for us. The second sensor that was ordered and tested is a simple float switch (Figure A8). The switch is oriented in such a way that when there is no water present the circuit is incomplete. When water is present it raises the buoyant float thus completing the circuit. We have shown that this sensor works in both tap water and demineralized water.

With the sensor decided upon, a Raspberry Pi microcomputer that can operate without human supervision and uses very little power, was sourced and installed with the lightest version of the operating system. We used the Python programming language to enable the detection and warning functions in Raspberry Pi microcomputer.

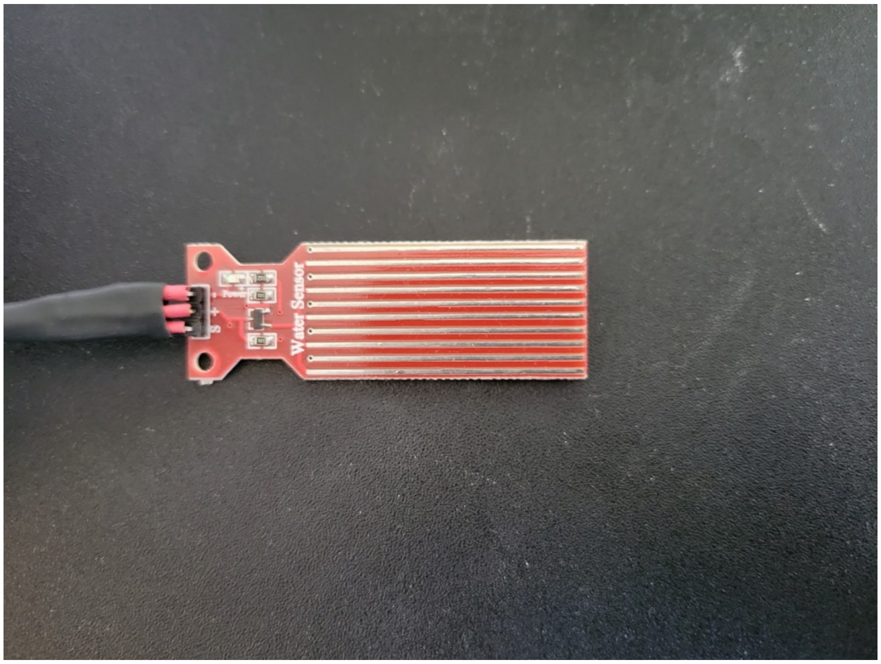

FIG. A7. A water level sensor to detect water on the laboratory floor in case of tank failure.

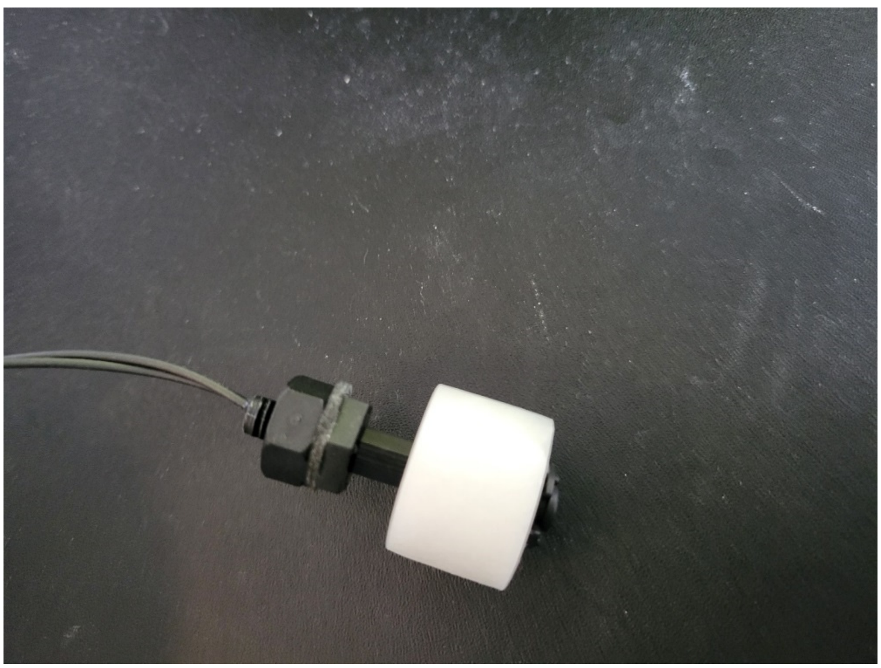

FIG. A8. A float-type sensor/switch that works with any liquid more dense than the float. The float is the white component in the picture.

In the final step, we must source a pump capable of quickly emptying water inside the berm area. The pump should be self-priming, as normally it would be dry. A promising choice is a pump (used in recreational vehicles and large boats) that can flow 17 litres per minute. If the tank failed and started filled the berm, this pump could completely drain 543 litres (the volume in a fully-filled tank) in about 32 minutes.

PART B: TRANSDUCERS

Water-filled tanks are used for scale modelling of seismic acquisition in marine environments. We characterized the wavelet shapes and 2D radiation/reception patterns of three types of immersion piezoelectric transducers: Dynasen CA-1136 piezopins, GS300F256M low-frequency specialty transducers from Ultran Corporation, and Murata PKM13EPYH4004-B0 commercial buzzers.

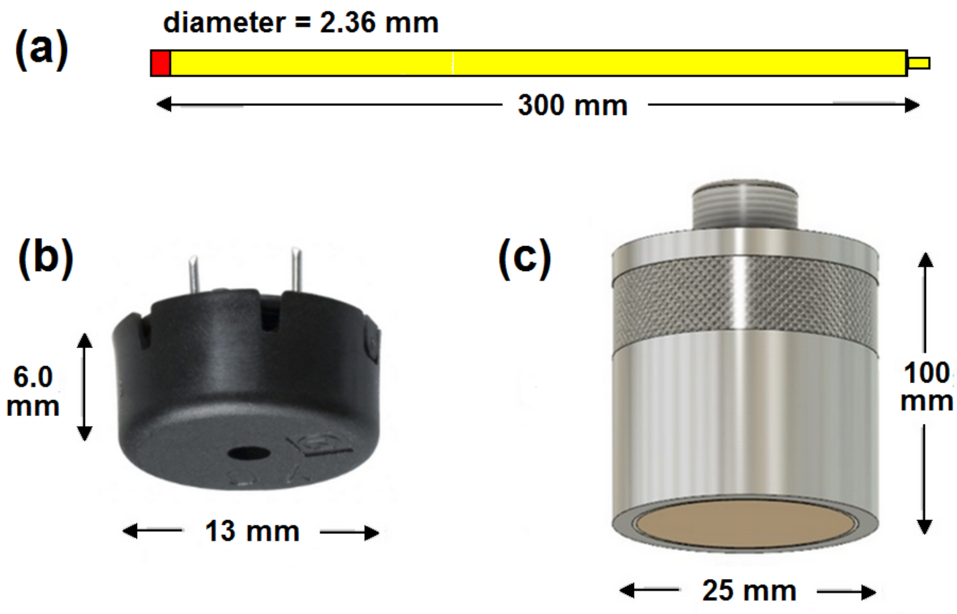

FIG. B1. Piezoelectric transducers used to create physical ultrasonic data potentially suitable for efficient FWI imaging. (a) Dynasen CA-1136 piezopin. (b) Murata PKM13EPYH4004-B0 buzzer. (c) Ultran GS30-D25 transducer. Dominant frequencies of the source-receiver signatures are roughly inversely proportional to their diameters.

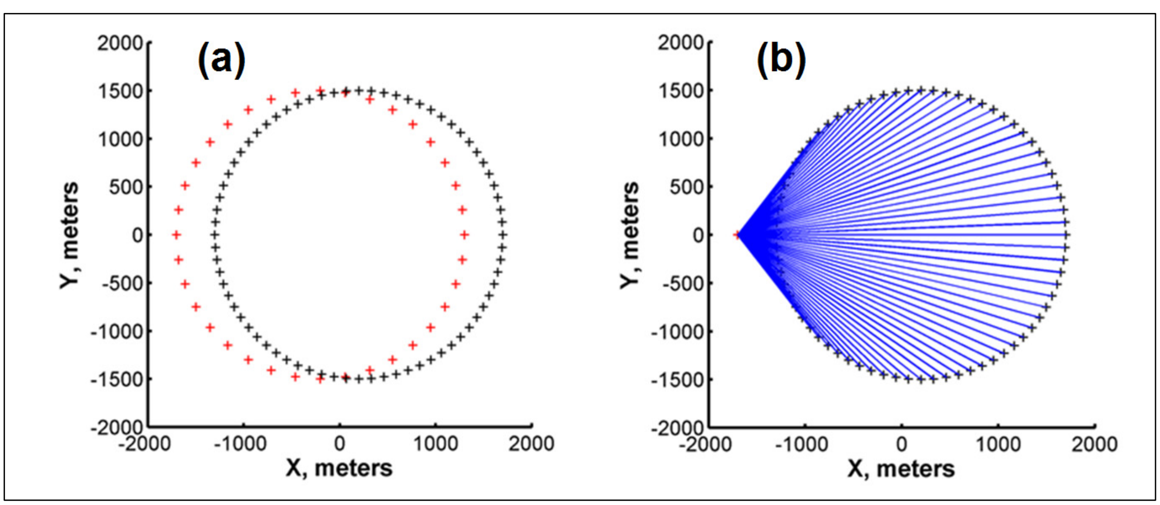

FIG. B2. (a) Source (red) and receiver (black) locations. (b) Raypaths for acquiring sample data. The dimensions shown have been scaled up from laboratory values.

Using pairs of identical transducers as source and receiver immersed in water, we recorded ultrasonic data using the geometric configuration depicted on Figure 2. All dimensions and frequencies stated in this report have been scaled by factor 10^4 to conform seismic exploration parameters. Hence, in reality, a stated seismic exploration length of 1m is a laboratory length of 0.1mm, and a seismic frequency of 1Hz is an ultrasonic frequency of 10 kHz, Sample seismograms acquired with piezopins, buzzers, and Ultran transducers, are plotted on Figures B3, B4, and B5, respectively.

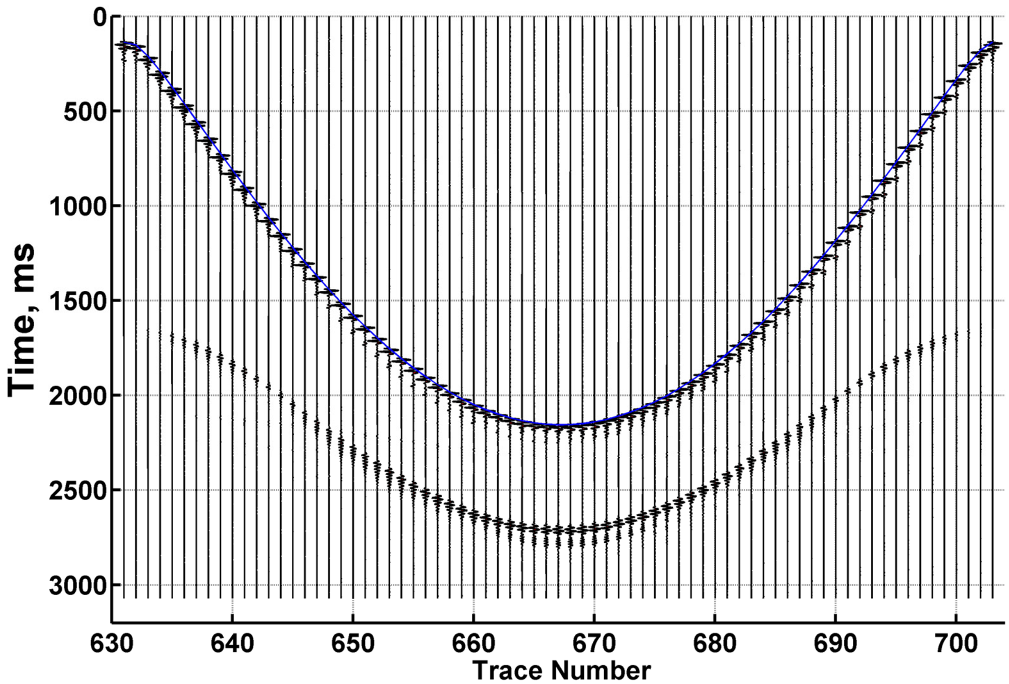

FIG. B3. Trace-normalized displays of example raw seismograms acquired using Dynasen piezopins. Dominant wavelet frequency is about 50Hz.

The CSG seismograms acquired with piezopin transducers displayed on Figure B3 exhibit short-duration wavelets with dominant frequency near 50Hz (500kHz unscaled). The short duration and high frequency increases the resolution capability for imaging using standard migration techniques. But the high frequency makes FWI imaging inefficient because the Finite Difference (FD) forward modelling steps require very fine grid sizes and small time steps. The event beneath the first arrivals is the reflection from the water-air interface.

The CSG seismograms acquired with buzzer transducers displayed on Figure B4 show wavelets with dominant frequency near 7Hz (70kHz unscaled) and coda with reasonably short duration. The moderately low frequency and moderately short duration makes the buzzer-acquired data suitable for efficient FWI imaging, provided that the wave shapes remain consistent as source-receiver positions vary. The event beneath the first arrivals is the reflection from the water-air interface.

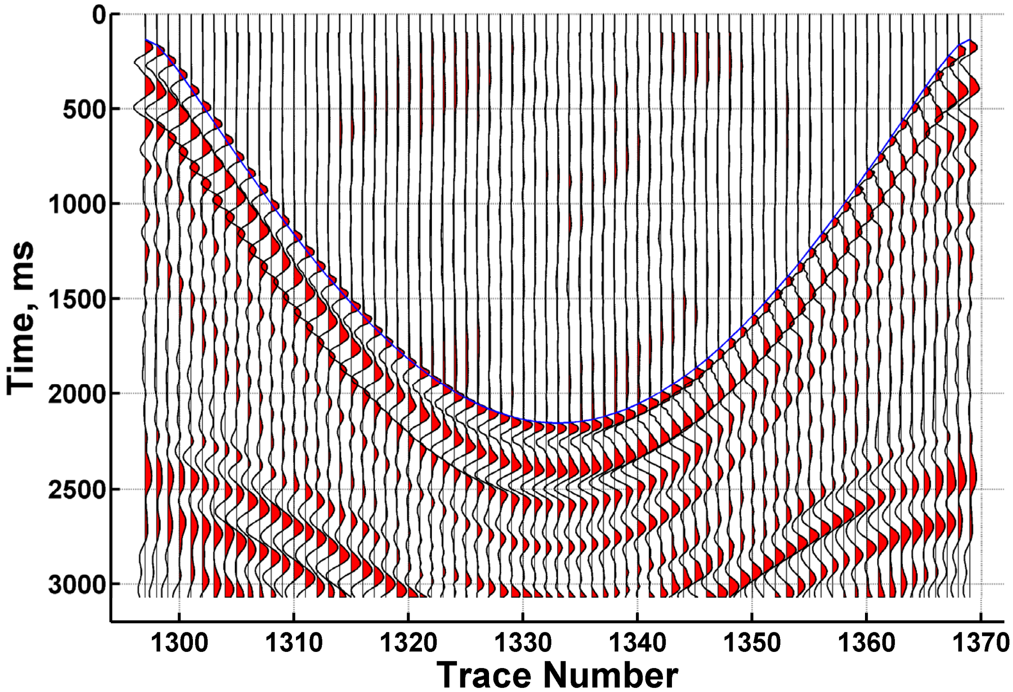

FIG. B4. Trace-normalized display of example raw seismograms acquired using buzzer transducers. Dominant wavelet frequency is about 7Hz (70kHz unscaled)

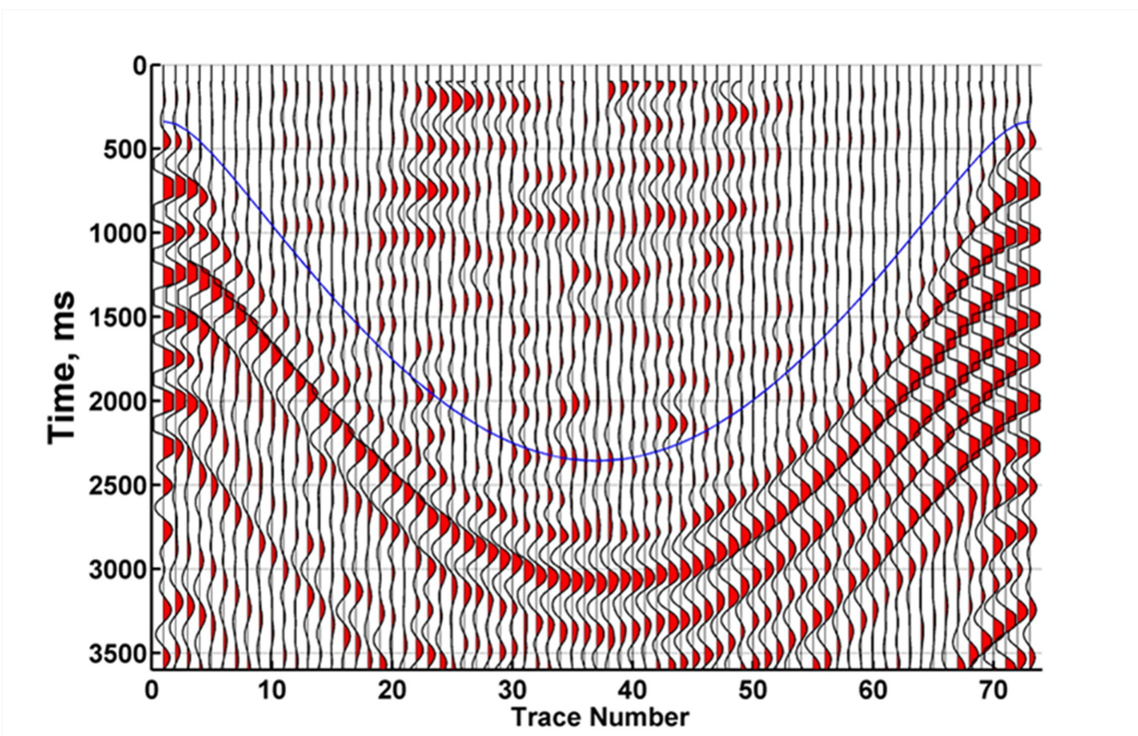

FIG. B5. Trace-normalized display of example raw seismograms acquired with Ultran low-frequency transducers. Dominant wavelet frequency is about 3Hz (30kHz unscaled)

Figure B5 displays CSG seismograms acquired with the low-frequency Ultran transducers. The traces here have a dominant frequency on order of 3Hz (30kHz unscaled). The dominant wavelength in water is about 30m (0.050m unscaled). The SNRs on the seismograms are not good, and the wavelet time-durations are even longer than those for the buzzer-acquired data. Most of the noise is due to reverberations within the water volume and especially to multiple reflections between the water-air interface and the bottom of the tank.

The long-duration coda and high noise levels are waveform characteristics are very poor in terms of suitability for use in FWI imaging, or in truth for any type of seismic imaging. We therefore dismiss any further use of the Ultran transducers for physically modelling by CREWES.

Piezopin-acquired signals vs buzzer-acquired signals

On Figures B6 and B7, we compare the signals produced by piezopin and buzzer transducers. The piezopin-acquired traces (Figure B6) exhibit wavelets with high dominant frequencies and short time durations. Both characteristics make these data effective for high-resolution imaging via traditional migration methods. But the high dominant frequencies work against efficient FWI imaging using commonly available computers, because the required small grid sizes and small time steps in iterative finite difference modelling lead to unacceptably long run-times. However, on supercomputers or on platforms using very fast GPU processors (Trad, 2021), FWI with piezopin-acquired data would be viable.

The buzzer-acquired signals (Figure B7) have a dominant frequency of about 7Hz. The wavelength in water is about 7 seven times greater than the wavelength of the 50Hz piezopin-acquired signals. For iterative finite difference modeling in two dimensions, spanning a fixed area with a given length of seismic traces, the larger wavelength and lower frequency gives an run-time advantage of about 343 (7x7x7) over that for the higher-frequency piezopin-acquired data. A rough rule of thumb is that the efficiency of FWI is inversely proportional to the cube of the dominant frequency in the input data. This is why we seek transducers producing source wavelets with lower dominant frequencies (but still with adequately short time durations).

Time-lapse results

Figures B7 and B8 show sample CSGs from the baseline survey and the monitor survey of a time-lapse experiment. The seismograms on Figure B7 were recorded through a circular area in a homogeneous volume of water, while the seismograms on Figure B8 were recorded after two targets were placed within the circumference of the circle. The same acquisition geometry was used in both cases. Evidence for the existence of targets can be seen in the differences between the two CSGs. Despite some inevitable experimental shortcomings in the data, Keating and Innanen (2022, this volume) have used the full datasets (each comprising of 2665 seismic traces) to conduct successful FWI imaging of the two targets.

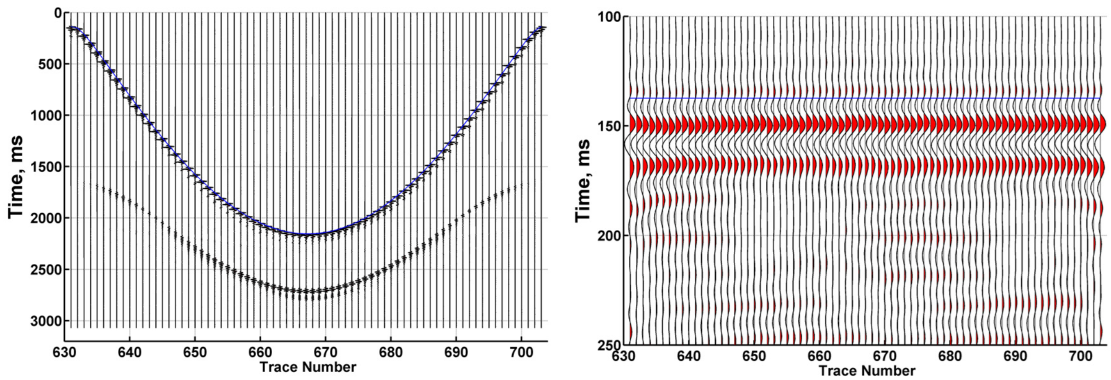

FIG. B6. Trace-normalized displays of example piezopin-acquired data. Left: Unprocessed traces, saved in file pzp_400HV_40dB_NoTarget.sgy. Right: Pre-processed and aligned traces show repeatable wave shapes as source-receiver positions vary. Wavelet duration is less than 50ms.

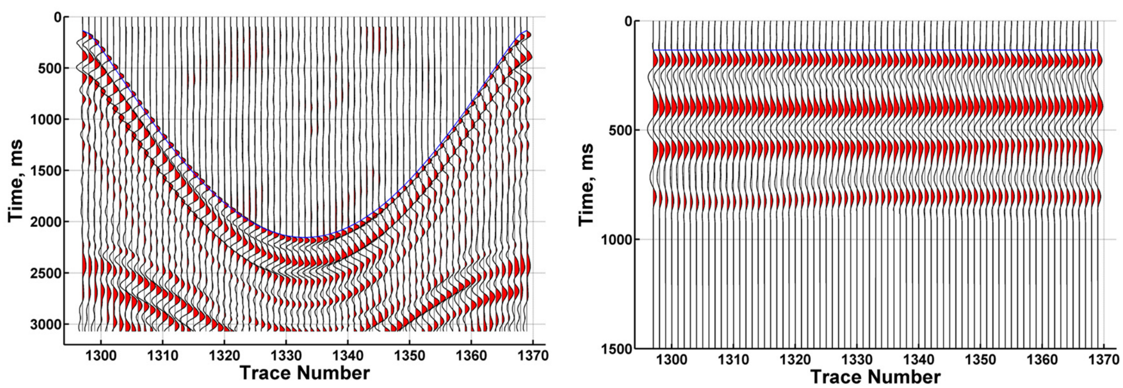

FIG. B7. Trace-normalized displays of buzzer-acquired data in a target-free medium. Left: Unprocessed traces, saved in file bzzrH_40dB_NoTarget.sgy. Right: Pre-processed traces, flattened to first-break times and showing repeatable wavelet shapes. The repeatability is specific to this particular transducer orientation in the X-Y plane. The wavelet duration is about 700ms.

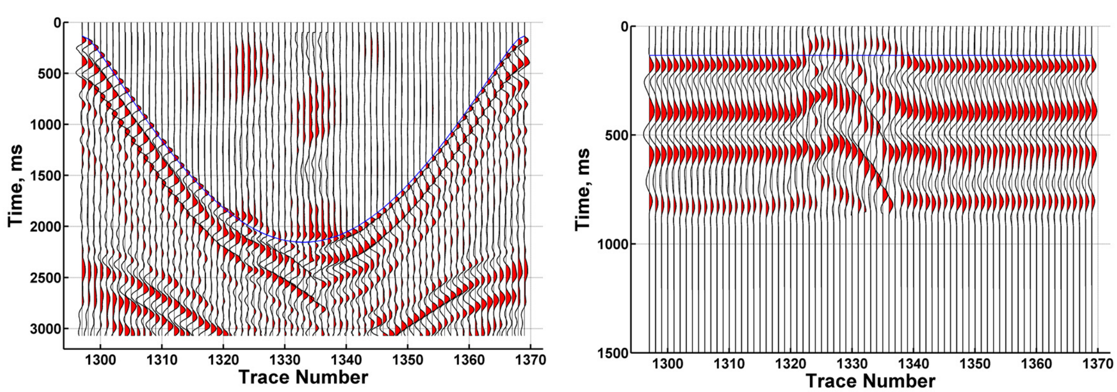

FIG. B8. Trace-normalized display of traces acquired in a medium with two targets. Left: Unprocessed traces, saved in file bzzrH_40dB_RingPCV.sgy. Right: Pre-processed traces, flattened to first break (water arrival) times. There is clear evidence for presence of the targets.

Although the examples of buzzer-acquired CSGs on Figures B7 and B8 show consistent wavelet shapes, this is not always the case. The wavelet shapes of data acquired with buzzer transducers depend on the orientation of buzzers. Repeatability does not hold if the transducers are rotated about the Z-axis from the specific angles employed for the data on Figures B7 and B8.

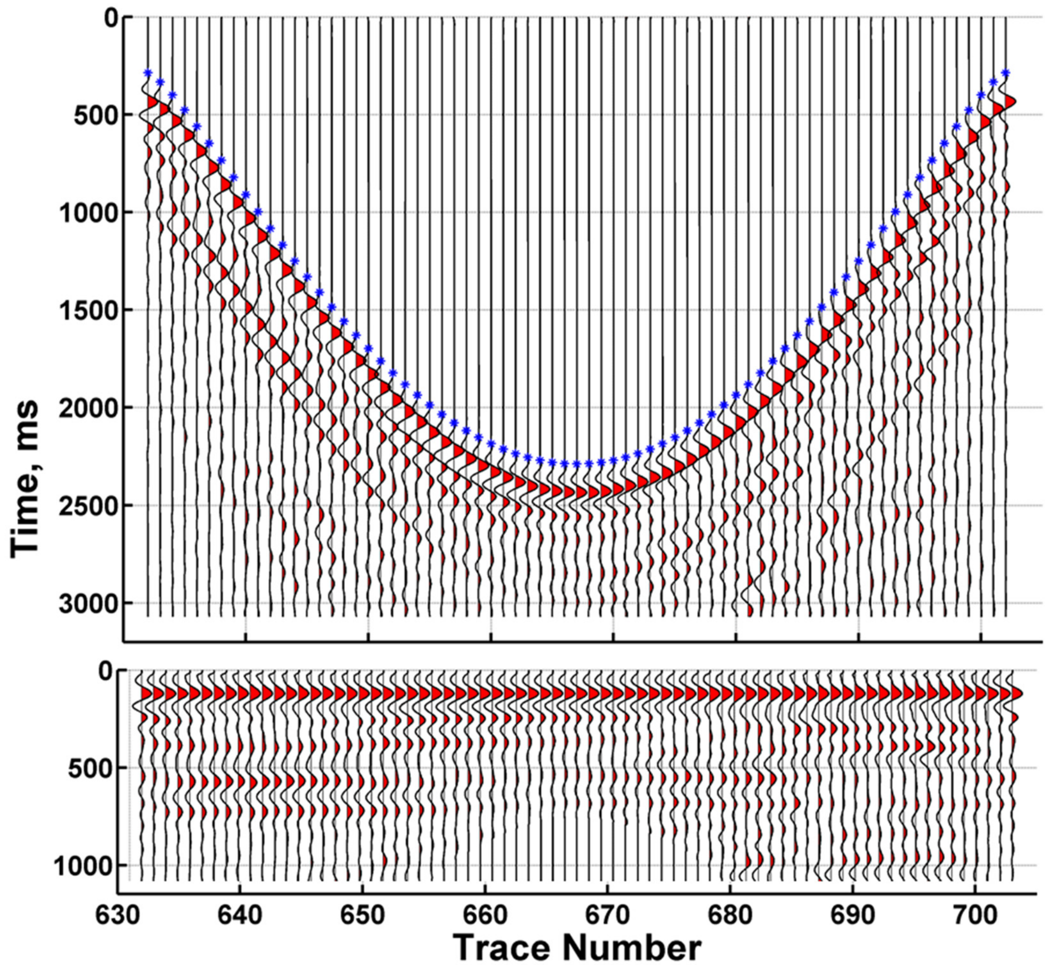

FIG. B9. An example CSG of buzzer-acquired seismograms that do not exhibit consistent wavelet shapes as source-receiver position vary.

Figure B.9 shows a CSG of buzzer-acquired seismograms recorded with the buzzers mounted with an orientation that does not yield consistent wavelet shapes. We can see that, for both the unaligned and aligned traces, the wavelets change quite noticeably as source-receiver positions change.

In the experiments, buzzers are mounted so that their external footprints in the X-Y plane are circular and symmetric. But there are asymmetries in the internal construction of the buzzers. These cause their radiation-reception patterns to be asymmetric in the X-Y plane. This in turn leads to inconsistent wavelet shapes for different source-receiver positions. We will try to fix this issue in the future.

PART C: ARBITRARY WAVEFORM GENERATOR

Real-world seismic exploration use sources that produce different source waveforms. Examples are impulsive dynamite explosion, timed explosions to yield consecutive impulses, and Vibroseis signals with a variety of control parameters (i.e., sweep lengths, frequency limits and tapers, low-dwell emphasis, linear or non-linear sweeps).

We wish to have the ability in physical modelling to drive the source transducers with controlled wave shapes. The ability to produce controlled source-waveforms would increase the types of seismic physical-modeling experiments that are possible. Piezoelectric transducers driven by these controlled waveforms can be used in simulations of real-world seismic sources such as swept-frequency vibrators, impulsive sources with controlled delay times, and complex SWD signals produced by drill-bits interacting with subsurface rocks. For this purpose, we have designed and built a prototype Arbitrary Waveform Generator (AWG). The heart of the AWG is a Raspberry Pi 4B microcomputer driving an R2R resistor ladder for digital-to-analogue conversion.

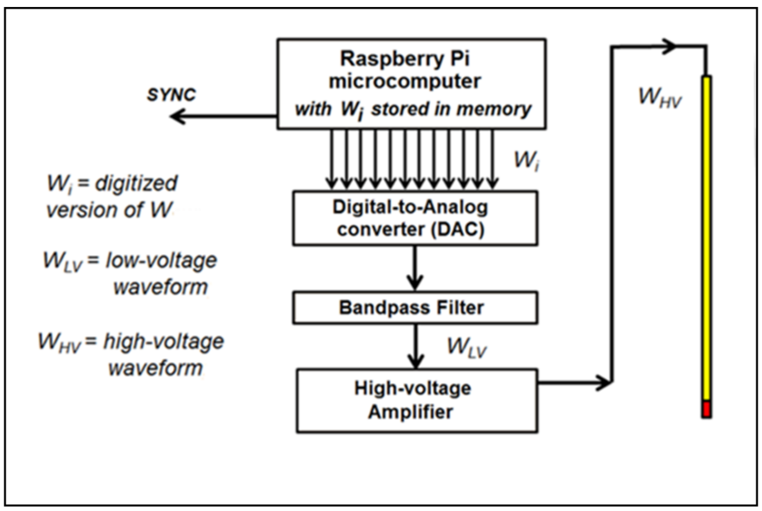

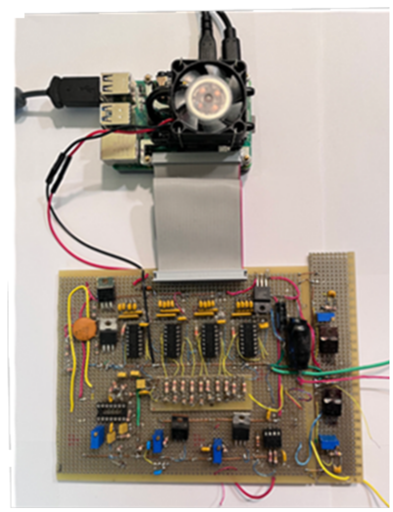

FIG. C1: Left: Block diagram of the arbitrary waveform generator (AWG) for driving piezoelectric source transducers. *W* is the desired waveform; both W_{LV} and W_{HV} are analog signals. Right: Raspberry PI Model 4B with prototype AWG support circuit board.

The input data for Figure C3 are floating point numbers stored in ASCII files. Raspberry software reads the numbers, normalizes and level-adjusts them, and then converts them to 9-bit integers so that the minimum and maximum amplitudes fall in the range of 0 to 511. The converted digital numbers are sent at a sample rate of 1 to 2 samples every microsecond to the R2R ladder whose output is an analog version. This analog signal is amplified to a desired level to drive a piezoelectric source transducer.

The test example shown on Figures C3(a) and C(b) indicates that, the AWG produces an output signal that preserves both amplitude and timing of the input waveform quite well, with only minor distortion between the input and output waveforms.

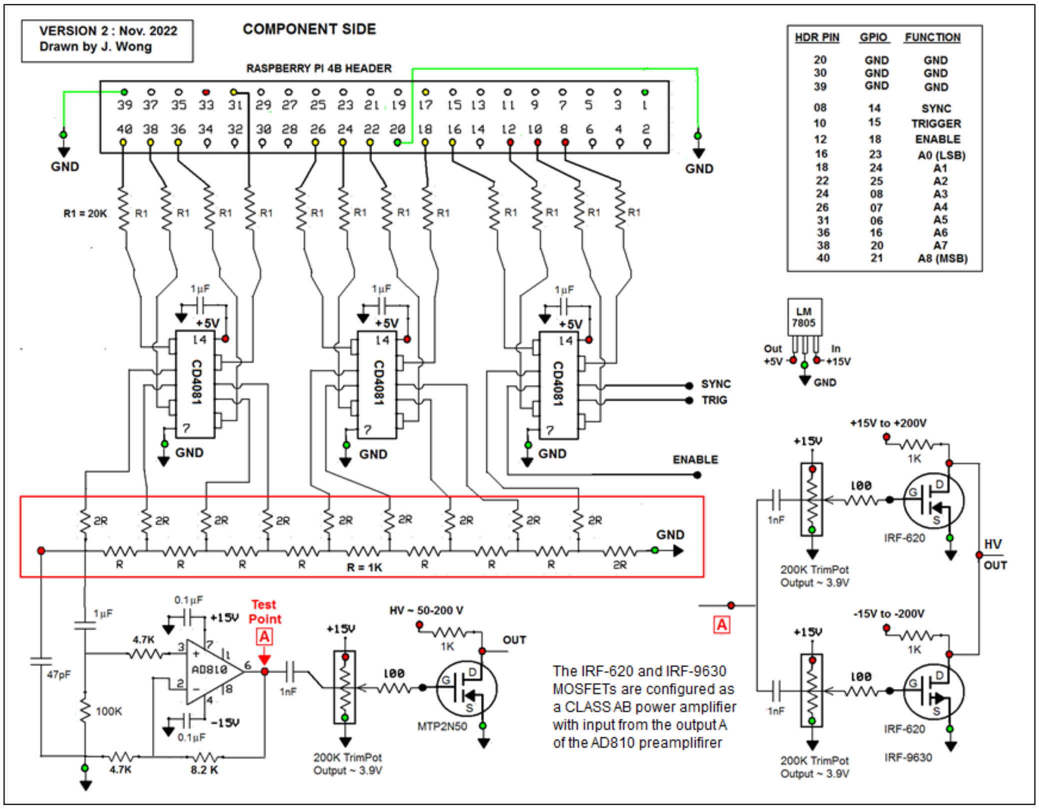

FIG. C2. Schematic diagram for the circuit design of the AWG prototype board. It shows the layout of electronic components and integrated circuits (ICs) and how they are connected.

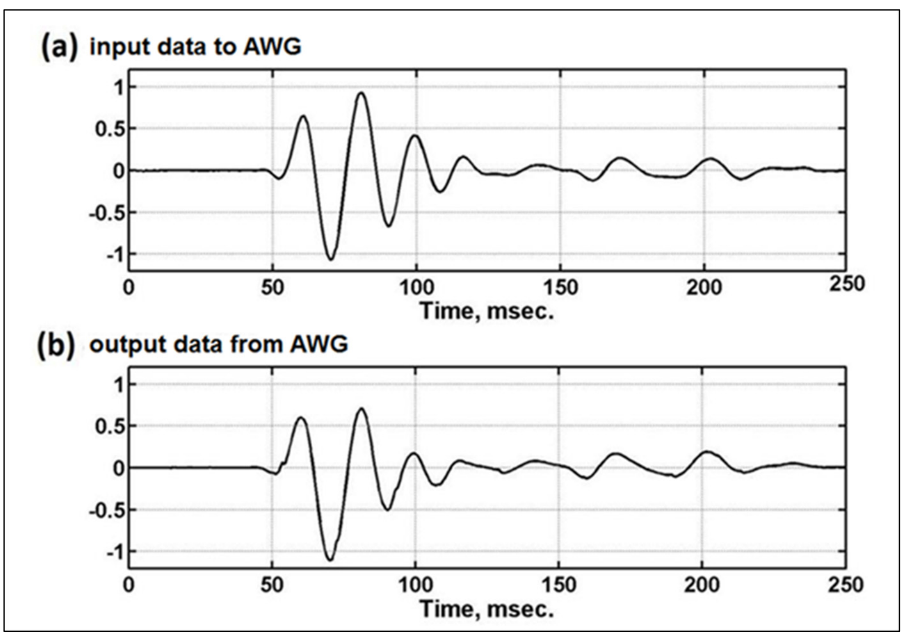

FIG. C3: (a) Input data to AWG (piezopin impulse response, stored on file as digitized numeric data); (b) Analog output from the AWG taken at Test Point A on Figure C2, as digitized by a Gage 4424 ADC module.

CONCLUSION

The new water tank constructed with reinforced acrylic sides has held up under water pressure (with no bowing of sides or leaks) continuously for more than 100 days to date. It should be capable of long-term use without failure, but just in case if there is such a failure, we intend to implement a flood mitigation system. This will consist of a berm on the floor under the positioning gantries, a water-detecting switch to start a pump to bail any water within the berm, and a continuously running Raspberry Pi microcomputer programmed to notify key personnel via email if water from leaks or a flood is detected.

Studies of wavelet shapes and radiation/reception patterns of the three types of transducers showed that piezopins produced the most consistent wavelet shapes with the shortest time durations and the most symmetric radiation patterns. However, the dominant frequency of the observed wavelets (about 50Hz, or 500kHz unscaled) is considered too high for efficient FWI imaging using commonly available computational devices. However, on computers based on fast GPU processors (Trad, 2021), FWI using such high-frequency seismic data should be viable.

The dominant frequency of data recorded with Murata buzzers is about 7Hz (70kHz unscaled). Wavelet shapes and radiation patterns recorded with the Murata buzzers seem to be dependent to mounting details. For a specific orientation, we have observed highly repeatable wavelets. A changed orientation yields inconsistent wavelets that vary with source-receiver positions. Despite these issues, Keating and Innanen (2021, this volume) applied FWI to a set of time-lapse transmission seismograms (acquired using buzzers mounted in that specific orientation) and obtained credible 2D images.

The wavelets from the Ultran specialty transducers have dominant frequencies near 3Hz (30kHz unscaled). The coda is very long and not repeatable for different source-receiver positions. The radiation-reception lobes are very strong in the Z-direction. They result in large-amplitude reflections bouncing between the water-air interface and the tank bottom and noise interfering with events of interest. For these reasons, the Ultran transducers will have only limited use in our Physical Modelling System.

We designed and produced an Arbitrary Waveform Generator and evaluated its use for producing source-driving functions more complicated than simple impulses. In the near future, we will use these complex source-driving waveforms to acquire complete sets of physically-modelled seismic data.

ACKNOWLEDGEMENT

This work was funded by the industrial sponsors of the (CREWES), by the NSERC grants CRDPJ 461179-13 and CRDPJ 543578-19.

REFERENCES

Keating, S., and Innanen, K.A, 2022 (this volume), Cross-gradient regularization for multiparameter FWI of physically modelled data, CREWES Research Reports, **34**, 30.

Trad, D. O., 2021, GPU applications for modelling, migration, inversion, and machine learning, CREWES Research Reports, **33**, 45.